Research Letter DOI: 10.15541/jim20240091

Mechanical Properties and Thermal Shock Resistance of $SrAl_2Si_2O_8$ Reinforced BN Ceramic Composites

WANG Bo[1,2], CAI Delong[1], ZHU Qishuai[2,3], LI Daxin[2], YANG Zhihua[2], DUAN Xiaoming[2], LI Yanan[4], WANG Xuan[5], JIA Dechang[2], ZHOU Yu[2,6]

(1. International Joint Laboratory of Advanced Nanomaterials of Heilongjiang Province, College of Materials Science and Chemical Engineering, Harbin Engineering University, Harbin 150001, China; 2. Key Laboratory of Advanced Structural-Functional Integration Materials, School of Materials Science and Engineering, Harbin Institute of Technology, Harbin 150001, China; 3. China Resources Cement Technology R&D Co., Ltd, Guangzhou 510000, China; 4. The First Military Representative Office of the Army Equipment Department in Beijing, Beijing 100072, China; 5. The Fourth System Design Department, Fourth Academy, China Aerospace Science and Industry Corporation Limited, Beijing 100048, China; 6. School of Materials Science and Engineering, Harbin Institute of Technology (Shenzhen), Shenzhen 518055, China)

Abstract: Hexagonal boron nitride (*h*-BN) ceramics have become exceptional materials for heat-resistant components in hypersonic vehicles, owing to their superior thermal stability and excellent dielectric properties. However, their densification during sintering still poses challenges for researchers, and their mechanical properties are rather unsatisfactory. In this study, $SrAl_2Si_2O_8$ (SAS), with low melting point and high strength, was introduced into the *h*-BN ceramics to facilitate the sintering and reinforce the strength and toughness. Then, BN-SAS ceramic composites were fabricated *via* hot press sintering using *h*-BN, $SrCO_3$, Al_2O_3, and SiO_2 as raw materials, and effects of sintering pressure on their microstructure, mechanical property, and thermal property were investigated. The thermal shock resistance of BN-SAS ceramic composites was evaluated. Results show that phases of as-prepared BN-SAS ceramic composites are *h*-BN and *h*-$SrAl_2Si_2O_8$. With the increase of sintering pressure, the composites' densities increase, and the mechanical properties shew a rising trend followed by a slight decline. At a sintering pressure of 20 MPa, their bending strength and fracture toughness are (138±4) MPa and (1.84±0.05) MPa·$m^{1/2}$, respectively. Composites sintered at 10 MPa exhibit a low coefficient of thermal expansion, with an average of 2.96×10^{-6} K^{-1} in the temperature range from 200 to 1200 ℃. The BN-SAS ceramic composites prepared at 20 MPa display higher thermal conductivity from 12.42 to 28.42 $W\cdot m^{-1}\cdot K^{-1}$ within the temperature range from room temperature to 1000 ℃. Notably, BN-SAS composites exhibit remarkable thermal shock resistance, with residual bending strength peaking and subsequently declining sharply under a thermal shock temperature difference ranging from 600 to 1400 ℃. The maximum residual bending strength is recorded at a temperature difference of 800 ℃, with a residual strength retention rate of 101%. As the thermal shock temperature difference increase, the degree of oxidation on the ceramic surface and cracks due to thermal stress are also increased gradually.

Key words: BN matrix composite; hot-press sintering; mechanical property; thermal shock resistance; service reliability

Vehicle radomes are important structural components located at the front end of a vehicle to reduce air resistance, maintain aerodynamic shape and protect the effective transmission of electromagnetic wave signals

Received date: 2024-03-03; **Revised date:** 2024-05-09; **Published online:** 2024-05-16
Foundation item: National Natural Science Foundation of China (52072088, 52072089); Natural Science Foundation of Heilongjiang Province (LH2023E061); Scientific and Technological Innovation Leading Talent of Harbin Manufacturing (2022CXRCCG001); Fundamental Research Funds for the Central Universities (3072023CFJ1003)
Biography: WANG Bo (1996–), male, PhD candidate. E-mail: bowang6600@126.com
王 博(1996–), 男, 博士研究生. E-mail: bowang6600@126.com
Corresponding author: CAI Delong, associate professor. E-mail: dlcai@hit.edu.cn; JIA Dechang, professor. E-mail: dcjia@hit.edu.cn
蔡德龙, 副教授. E-mail: dlcai@hit.edu.cn; 贾德昌, 教授. E-mail: dcjia@hit.edu.cn

and efficient communication[1]. In flight, the radome endures intense aerodynamic heating and loads[2], as well as particle erosion[3]. Simultaneously, the radome is expected to exhibit excellent wave transparency to ensure normal radar operation during high-speed flight[4-5]. Therefore, vehicle radome materials must possess excellent comprehensive performance of heat protection-carrying-wave transmission-integration.

Hexagonal boron nitride (*h*-BN) possesses a crystal structure similar to that of graphite[6]. The special crystal structure endows *h*-BN with a series of unique comprehensive properties[7-10], such as low dielectric coefficient (3–5), low loss tangent ($(2\times10^{-4}–8\times10^{-4})$), extremely high sublimation temperature of about 3000 ℃ (in non-oxidative atmosphere), chemical inertness, excellent thermal shock resistance, tribological properties and good machining performance[11]. Consequently, it is an excellent material for preparing vehicle radome.

However, the strong covalent bond structure of *h*-BN hints its sintering and densification because of its minimal solid diffusion coefficient. Therefore, researchers have facilitated sintering by introducing a secondary phase that creates a liquid phase during sintering, such as SiO_2-BN[12], BN-MAS[13-14], BN-Y_2SiO_5[15], BN-Y_2O_3-AlN[16], BN-La-Al-Si-O[17], BN-YAG[18], AlN-*h*-BN[19], and BN-SiC[20].

In this study, BN-SAS ceramic composites were fabricated by hot-press sintering. $SrAl_2Si_2O_8$ (SAS) exhibits excellent mechanical properties, with high bending strength (134 MPa), low dielectric constant (~9.0), and low melting point (~1675 ℃)[21-22], which is expected to improve the comprehensive performance of BN ceramics. Effects of sintering pressure on the microstructure, mechanical properties, and thermal properties of BN-SAS ceramic composites were investigated. The thermal shock resistance and thermal shock damage mechanism of BN-SAS ceramic composites were also discussed.

1 Experimental procedures

1.1 Manufacturing process

The starting raw materials included *h*-BN powders (d_{50}=1.31 μm, 99% purity, Dandong Chemical Research Institute Co., Ltd., China), $SrCO_3$ powders (d_{50}=3.12 μm, 99% purity, Tianjin Guangfu Fine Chemical Research Institute, China), Al_2O_3 powders (d_{50}=0.72 μm, 99% purity, Taimei Chemicals Co., Ltd., Japan), and SiO_2 powders (d_{50}=3.39 μm, 98% purity, Lianyungang Guangyu Quartz Products Co., Ltd., China). $SrCO_3$, Al_2O_3 and SiO_2 were combined in the stoichiometric ratio required to yield $SrAl_2Si_2O_8$. SAS was added with mass fraction of 30%, which was roughly equivalent to a volume fraction of 23%.

The starting powders were ball-milled in anhydrous ethanol for 24 h. Subsequently, the powder mixtures were hot-pressed in a 50 mm diameter mold, illustrated in Fig. 1, at 1800 ℃ for 60 min under a pressure range of 10~30 MPa in 1.013×10^5 Pa N_2 atmosphere.

1.2 Thermal shock experiment

The water-quenching method was chosen to investigate the thermal shock resistance of the BN-SAS ceramic composites. The muffle furnace temperatures were set to target temperatures of 625, 825, 1025, 1225 and 1425 ℃. The samples were inserted into the furnace and held for 10 min to obtain a uniform temperature distribution, respectively. After heat preservation, the samples were promptly quenched in water against temperature difference ΔT of 600, 800, 1000, 1200 and 1400 ℃, respectively. The residual bending strength of the specimens was tested.

1.3 Characterization

The density of the BN-SAS composite was measured in distilled water by the Archimedes principle (DV314C) at room temperature. The phase composition was determined *via* X-ray diffractometry (XRD, D/max-γB, Japan). The microstructural features of the samples

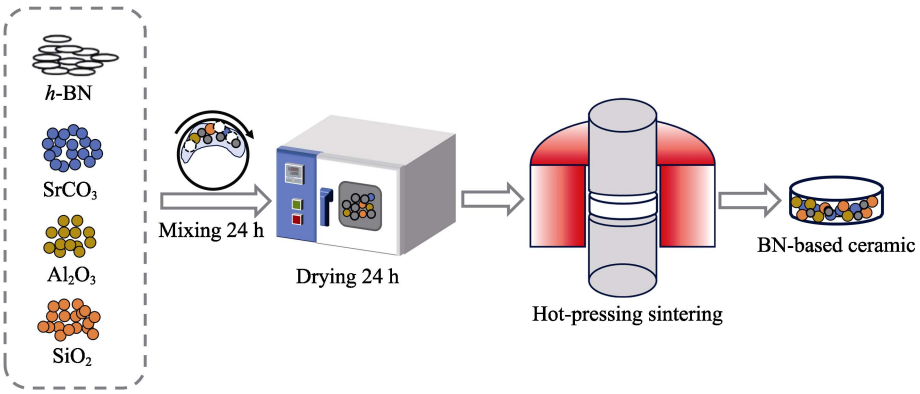

Fig. 1 Flow chart for the preparation of BN-SAS ceramic composites by hot-press sintering

were observed by scanning electron microscope (SEM, HELIOS NanoLab 600i, FEI, America and AMBER, TESCAN, Czech Republic). Microstructure and energy spectrum elemental analyses of composite samples were performed by using transmission electron microscope (TEM, Talos F200x, FEI, USA).

Bending strength was measured on sample with dimension of 3 mm×4 mm×36 mm by the three-point bending method. The fracture toughness (K_{IC}) was determined by the single-edge notched beam (SENB) method with specimen dimension of 2 mm×4 mm×25 mm, using an outer span of 16 mm fixture and a crosshead speed of 0.05 mm/min. Bending strength and fracture toughness values were the average of four measurements tested under the same condition. The loading direction was parallel to the direction of hot pressing. The modulus of elasticity was measured by the pulsed excitation method (RFDA-HTVP-1750 ℃, IMCE, Belgium).

Thermal conductivity of the ceramic composites was tested using laser thermal conductivity meter (LFA467HT, NETZSCH, Germany), in the range from 200 ℃ to 1000 ℃, carrying out parallel to the direction of hot pressing. The coefficient of thermal expansion (CTE) was measured using a thermal expansion meter (DIL402C, NETZSCH, Germany) over the temperature range from room temperature (RT) to 1200 ℃, carrying out perpendicular to the direction of hot pressing.

2 Results and discussion

2.1 Density and mechanical properties

Table 1 displays density, bending strength and fracture toughness of BN-SAS ceramic composites. The density of BN-SAS ceramic composites increases from 1.90 to 2.33 g/cm^3 with the sintering pressure increasing. This is primarily due to the low-melting SAS displaying a certain degree of mobility at the sintering temperature. Elevated sintering pressure enables the SAS liquid phase to spread more extensively and fill the pores more effectively.

The bending strength gradually increased with the increase of sintering pressure. SAS is more effective in facilitating sintering during the sintering process. When the sintering pressure reaches 20 MPa, the densification of the ceramic composites increases, resulting in a notable enhancement in bending strength. The fracture toughness of ceramic composites increases and then decreases with the increase of sintering pressure.

Table 1 Density, bending strength and fracture toughness of BN-SAS ceramic composites

Sintering pressure/ MPa	Density/ (g·cm^{-3})	Bending strength/ MPa	Fracture toughness/ (MPa·m$^{1/2}$)
10	1.90	87±5	1.33±0.04
20	2.25	138±4	1.84±0.05
30	2.33	136±11	1.50±0.24

2.2 Phase and microstructure

The main phases of the BN-SAS ceramic composites are *h*-BN and *h*-$SrAl_2Si_2O_8$ (Fig. 2), showing that Al_2O_3, $SrCO_3$ and SiO_2 in the pristine powder reacted stoichiometrically to form $SrAl_2Si_2O_8$. Additionally, under higher sintering pressure, $SrAl_2Si_2O_8$ exhibits stronger diffraction peaks, indicating that increasing the sintering pressure can promote the crystallization of strontium feldspar.

Fig. 3(a–c) present HRTEM images of BN-SAS ceramic composites sintered at 10 MPa. The *h*-BN grains show obvious lath-like features, and SAS is uniformly distributed within the pores of *h*-BN. The bond between the *h*-BN and SAS interfaces is tight and legible. The SAS comprises merely small crystalline grains that exhibit poor crystallinity, which is consistent with the XRD results. Adjacent to *h*-BN, the crystallinity of SAS surpasses that found in the interior regions. The interplanar spacing of BN crystal is measured at 0.33 nm, corresponding to the (002) crystal face of *h*-BN. The TEM image and elemental mappings are shown in Fig. 3(d–j). The interface between *h*-BN and SAS is also securely joined, without any obvious cracks or voids. The SAS phase is uniformly distributed within the pores of the “card room” structure formed by *h*-BN.

Fracture morphology is shown in Fig. 4. Fracture surface of the ceramic composites is uneven, featuring numerous lamellar particles resulting from the extraction of the plate-like *h*-BN particles from the matrix. The uneven fracture suggests a zigzag crack extension path, which absorbs fracture energy and enhances the bending

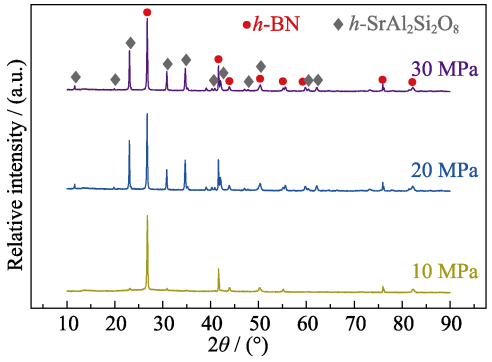

Fig. 2 XRD patterns of BN-SAS ceramic composites sintered at different pressures

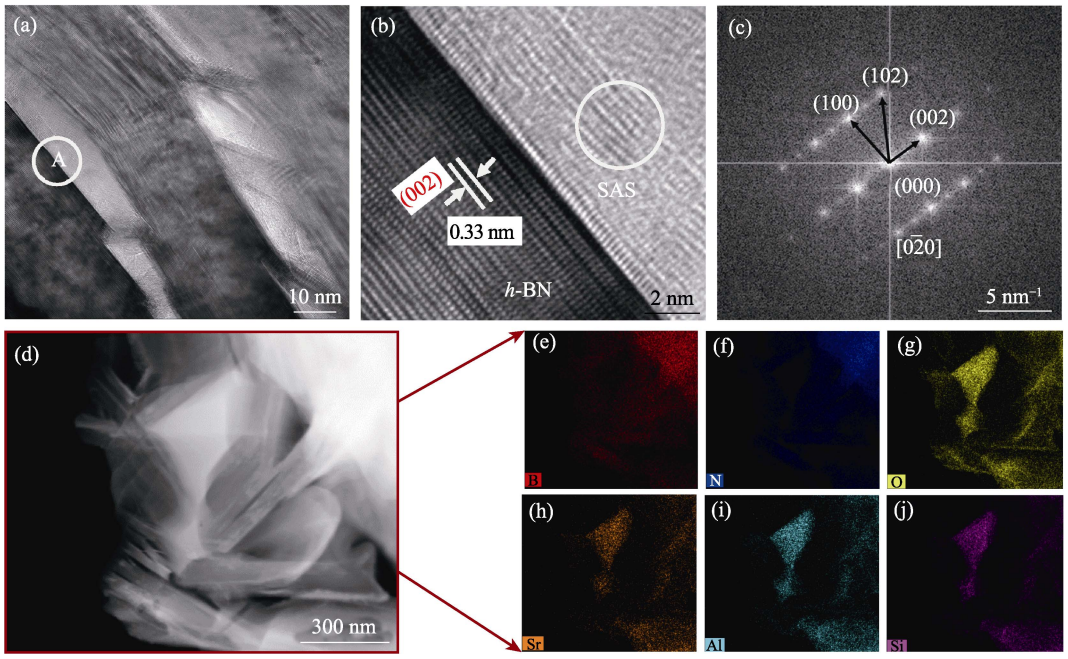

Fig. 3 HRTEM and TEM characterization of BN-SAS ceramic composites sintered at 10 MPa
(a) HRTEM image; (b) Inverse FFT image of area A in figure (a); (c) SAED pattern of *h*-BN; (d) TEM image of BN-SAS ceramic composites; (e-j) Elemental analysis of the figure (d); (e) B; (f) N; (g) O; (h) Sr; (i) Al; (j) Si

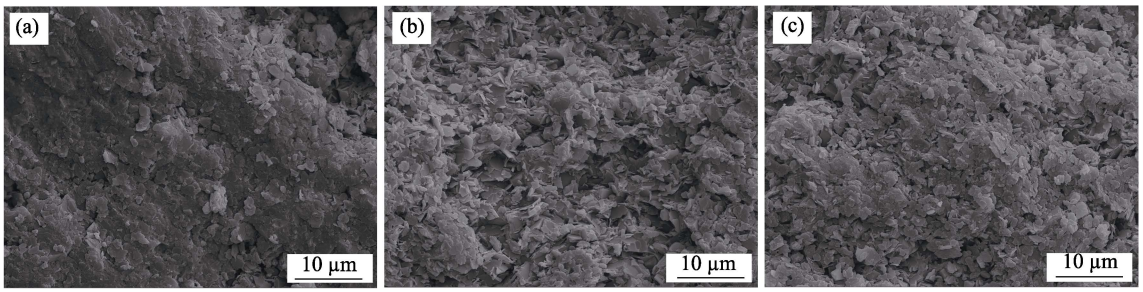

Fig. 4 Fracture microstructures of BN-SAS ceramic composites sintered at different pressures
(a) 10 MPa; (b) 20 MPa; (c) 30 MPa

strength. As the sintering pressure further increases, the fracture of the composites exhibits more denser morphology, with lamellar *h*-BN particles embedded within the secondary phase SAS.

2.3 Thermal properties and thermal shock resistance

Fig. 5(a) presents the temperature dependence of dL/L_0 of BN-SAS ceramic composites. The ratio dL/L_0 increases monotonically with the increase of temperature, maintaining a relatively uniform rate in the range of RT–600 ℃. At 1200 ℃, the value dL/L_0 peaks at 5.2×10^{-3}. These ceramic composites demonstrate positive coefficients of thermal expansion. The ceramic composites sintered at 20 MPa show the least dL/L_0 values, indicating minimal thermal expansion.

The inset in Fig. 5(a) displays the average CTE of BN-SAS ceramic composites over the temperature interval from 200 to 1200 ℃. The average CTE increases from 2.96×10^{-6} K^{-1} to 5.04×10^{-6} K^{-1} with the increase of sintering pressure. This is primarily because lowering the sintering pressure leads to higher porosity within the composites, which effectively accommodates the increased atomic spacing caused by atomic thermal vibrations, consequently reducing the CTE. In addition, the lowering sintering pressures remain the SAS primarily in an amorphous form, which further reduces the CTE.

Fig. 5(b) illustrates the thermal conductivity as a function of temperature. Thermal conductivity of ceramic composites increases slightly with sintering pressure rising in the range of RT–600 ℃, although the differences are minimal. In the range of 600–800 ℃, the thermal conductivity decreases with increased sintering pressure of 20 MPa and 30 MPa, and it is obviously lower than that of 10 MPa at 1000 ℃.

The mechanical and thermal properties of the ceramic composites were utilized to determine the thermal shock fracture resistance factor *R* and thermal shock damage factor R^{IV}[23-24], the outcomes are summarized in Table 2.

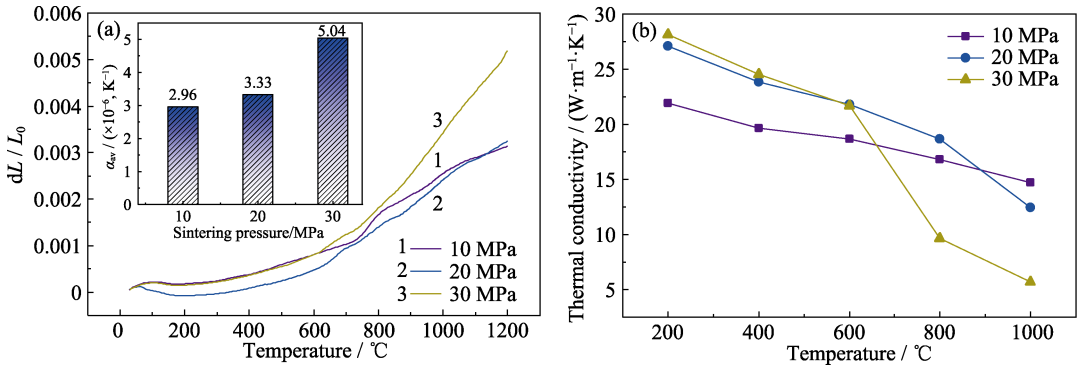

Fig. 5 Thermal properties of BN-SAS ceramic composites sintered at different pressures
(a) Thermal expansion rate with inset showing the average CTE (α); (b) Thermal conductivity

Table 2 Properties of the BN-SAS ceramic composites

Sintering pressure/MPa	Bending strength/MPa	Fracture toughness/ (MPa·m$^{1/2}$)	Young's modulus/GPa	Average CTE/ ($\times10^{-6}$, K^{-1})	λ/(W·m^{-1}·K^{-1}, 1000 ℃)	R/℃	R^{IV}/μm
10	87±5	1.33±0.04	48.47	2.96	14.70	609(1−ν)	230 / (1−ν)
20	138±4	1.84±0.05	67.83	3.33	12.42	613(1−ν)	177 / (1−ν)
30	136±11	1.50±0.24	66.94	5.04	5.72	404(1−ν)	122 / (1−ν)

ν : Poisson's ratio

At a sintering pressure of 20 MPa, the R reaches its maximum value, indicating that the ceramic composites exhibit the greatest critical thermal shock temperature difference and superior thermal shock resistance. Furthermore, the BN-SAS ceramic composites sintered at 20 MPa displayed the highest bending strength at room temperature. Consequently, the ceramic samples sintered at 20 MPa were selected for subsequent thermal shock resistance experiments.

The residual strength and residual strength rate of BN-SAS ceramic composites sintered at 20 MPa after thermal shock experiments with temperature differences ranging from 600 ℃ to 1400 ℃ are depicted in Fig. 6. The thermal shock residual strength of BN-SAS ceramic composites shows an initial increase followed by a decline with the increase of thermal shock temperature difference. The residual strength of the composite peaks is (140±15) MPa after the 800 ℃ thermal shock experiment, higher than that of unquenched samples. Subsequently, it decreases progressively with further increase in thermal shock temperature difference. This phenomenon is primarily due to the microstructure transformation of the composite.

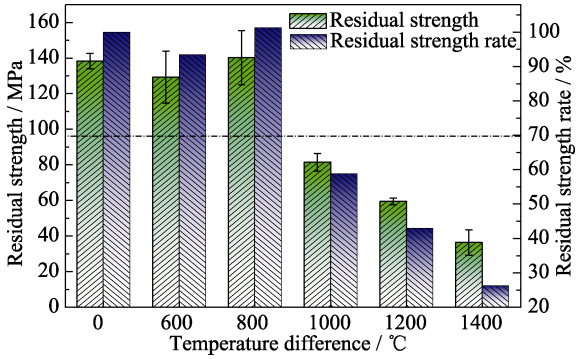

Fig. 6 Residual bending strength and residual strength rate of BN-SAS composites sintered at 20 MPa as a function of thermal shock temperature difference

The surface morphology of BN-SAS ceramic composites after thermal shock is shown in Fig. 7. With the thermal shock temperature difference gradually increasing, droplets and microcracks emerge on the surface of the ceramic composites. With the thermal shock temperature difference ranging from 600 ℃ to 800 ℃, a thin oxide layer forms on the surface of ceramic composites. The surface becomes smoother and denser, with a reduction in the number of pores. At this thermal shock temperature difference, the *h*-BN on the surface of the ceramic composite undergoes oxidation to form a mobile B_2O_3 liquid phase that encapsulates the surface and mends defects such as microcracks, enhancing the surface density of the samples.

When the thermal shock temperature difference reaches 1000 ℃, tiny glassy droplets appear on the surface of the ceramic composites. *h*-BN oxidizes to yield B_2O_3, that subsequently merges with SAS, resulting in formation of a stable and viscous SrO-Al_2O_3-SiO_2-B_2O_3 glass that adheres to the surface of the composite. Further increase in temperature difference exacerbates the oxidation process of *h*-BN, leading to a progressive enlargement of glassy droplets.

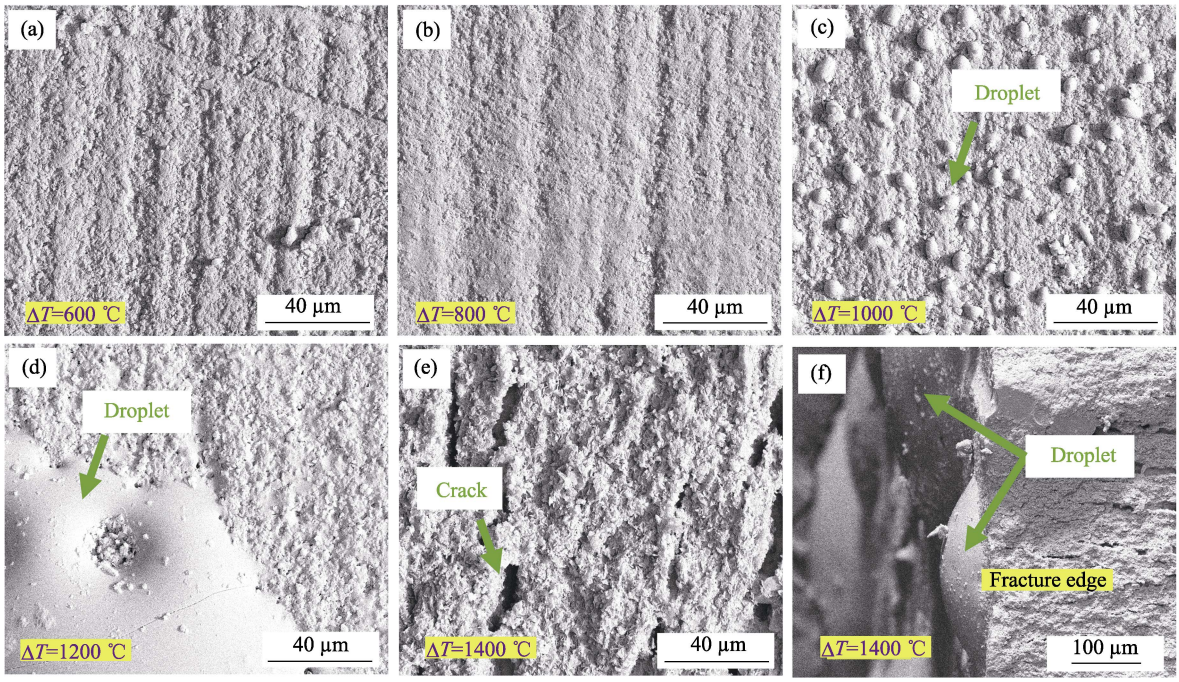

Fig. 7 Micrographs of surfaces and fracture edges of BN-SAS ceramic composites sintered at 20 MPa after thermal shock with different temperature differences

(a) 600 ℃; (b) 800 ℃; (c) 1000 ℃; (d) 1200 ℃; (e) 1400 ℃; (f) Fracture edge morphology under thermal shock temperature difference of 1400 ℃

At a thermal shock temperature difference of 1400 ℃, larger cracks appear on the surface of the ceramic composites. Numerous pores are evident, contributing to rough and uneven material surface. This indicates that the significant thermal stress inside the ceramic composites at this temperature difference causes material cracking, seriously diminishing the residual bending strength. Moreover, the enlargement of glassy droplets suggests a severe oxidation of the composites.

3 Conclusions

In this study, BN-SAS ceramic composites were prepared by hot-press sintering. Drawn from the experimental results and detailed microstructural analyses, conclusions are listed as follows.

1) The BN-SAS ceramic composites, fabricated by hot-press sintering, exhibit optimal mechanical properties at a sintering pressure of 20 MPa, with bending strength and fracture toughness of (138±4) MPa and (1.84±0.05) MPa·$m^{1/2}$, respectively.

2) The residual strength rate of BN-SAS ceramic composites after thermal shock at 800 ℃ was 101%. During thermal shock, the ceramic composites undergo oxidation, leading to the formation of a SrO-Al_2O_3-SiO_2-B_2O_3 glass film that encompasses on the surface of the composites, mending the surface defects and enhancing the mechanical properties of the BN-SAS composites.

References:

[1] KENION T, YANG N, XU C. Dielectric and mechanical properties of hypersonic radome materials and metamaterial design: a review. *Journal of the European Ceramic Society*, 2022, **42(1):** 1.

[2] KUMAR S, GUPTA P. A review on ceramic and polymer materials for radome applications. 2019 IEEE Indian Conference on Antennas and Propogation (InCAP), Ahmedabad, 2019.

[3] ADLER W. Development of design data for rain impact damage in infrared-transmitting windows and radomes. *Optical Engineering*, 1987, **26(2):** 262143.

[4] KHATAVKAR N. Composite materials for supersonic aircraft radomes with ameliorated radio frequency transmission—a review. *RSC Advances*, 2016, **6(8):** 679.

[5] KOZAKOFF D. Analysis of radome-enclosed antennas. Boston: Artech House, 1997.

[6] CI L J, SONG L, JIN C H, *et al*. Atomic layers of hybridized boron nitride and graphene domains. *Nature Materials*, 2010, **9(5):** 430.

[7] STEINBORN C, HERRMANN M, KEITEL U, *et al*. Correlation between microstructure and electrical resistivity of hexagonal boron nitride ceramics. *Journal of the European Ceramic Society*, 2013, **33(6):** 1225.

[8] WANG Z G, GE M, YU S Q, *et al*. Microstructural evolution of polymer-derived hexagonal boron nitride fibres under high-temperature stretching. *Journal of Advanced Ceramics*. 2023, **12(10):** 1973.

[9] EICHLER J, LESNIAK C. Boron nitride (BN) and BN composites for high-temperature applications. *Journal of the European Ceramic Society*, 2008, **28(5):** 1105.

[10] DING C, LIU G L. Preparation and mechanical properties of diamond/hexagonal boron nitride composite with spark plasma sintering. *Journal of Ceramics*, 2023, **44(3):** 517.

[11] WEI D, MENG Q C, JIA D C. Microstructure of hot-pressed

h-BN/Si_3N_4 ceramic composites with Y_2O_3-Al_2O_3 sintering additive. *Ceramics International*, 2007, **33(2):** 221.
[12] WEN G, WU G L, LEI T Q, *et al*. Co-enhanced SiO_2-BN ceramics for high-temperature dielectric applications. *Journal of the European Ceramic Society*, 2000, **20(12):** 1923.
[13] CAI D L, YANG Z H, DUAN X M, *et al*. A novel BN-MAS system composite ceramics with greatly improved mechanical properties prepared by low temperature hot-pressing. *Materials Science and Engineering: A*, 2015, **633:** 194.
[14] NIU B, CAI D L, YANG Z H, *et al*. Anisotropies in structure and properties of hot-press sintered *h*-BN-MAS composite ceramics: effects of raw *h*-BN particle size. *Journal of the European Ceramic Society*, 2019, **39(2/3):** 539.
[15] ZHANG X, CHEN J X, LI X C, *et al*. Microstructure and mechanical properties of *h*-BN/Y_2SiO_5 composites. *Ceramics International*, 2015, **41(1):** 1279.
[16] QIU B F, DUAN X M, ZHANG Z, *et al*. Microstructural evolution and mechanical properties of *h*-BN composite ceramics with Y_2O_3-AlN addition by liquid-phase sintering. *Rare Metals*, 2020, **39(5):** 555.
[17] QIU B F, DUAN X M, ZHANG Z, *et al*. Microstructural evolution of *h*-BN matrix composite ceramics with La-Al-Si-O glass phase during hot-pressed sintering. *Journal of Advanced Ceramics*, 2021, **10(3):** 493.
[18] ZHANG Z, DUAN X M, TIAN Z, *et al*. Texture and anisotropy of hot-pressed *h*-BN matrix composite ceramics with *in situ* formed YAG. *Journal of Advanced Ceramics*, 2022, **11(4):** 532.
[19] LIU Z T, ZHAO S Q, YANG T, *et al*. Improvement in mechanical properties in AlN-*h*-BN composites with high thermal conductivity. *Journal of Advanced Ceramics*, 2021, **10(6):** 1317.
[20] MIAO Y M, LIU L G. Effects of pressure and the content of SiC on densification and mechanical properties of hot press sintered *h*-BN ceramics. *Journal of Ceramics*, 2022, **43(4):** 637.
[21] CHINN R, HAUN M, KIM C, *et al*. Microstructures and properties of three composites of alumina, mullite, and monoclinic $SrAl_2Si_2O_8$. *Journal of the American Ceramic Society*, 2000, **83(11):** 2668.
[22] CHINN R, HAUN M, KIM C, *et al*. Low-temperature transient glass-phase processing of monoclinic $SrAl_2Si_2O_8$. *Journal of the American Ceramic Society*, 1998, **81(9):** 2285.
[23] YANG Z H, JIA D C, ZHOU Y, *et al*. Thermal shock resistance of *in situ* formed SiC-BN composites. *Materials Chemistry and Physics*, 2008, **107(2/3):** 476.
[24] HASSELMAN D. Thermal stress resistance parameters for brittle refractory ceramics: a compendium. *Ceramic Bulletin*, 1970, **49:** 1033.

$SrAl_2Si_2O_8$ 增强 BN 陶瓷的力学性能及抗热震性能

王 博[1,2], 蔡德龙[1], 朱启帅[2,3], 李达鑫[2], 杨治华[2], 段小明[2], 李雅楠[4], 王 轩[5], 贾德昌[2], 周 玉[2,6]

(1. 哈尔滨工程大学 材料科学与化学工程学院, 黑龙江省先进纳米材料联合实验室, 哈尔滨 150001; 2. 哈尔滨工业大学 材料科学与工程学院, 先进结构功能一体化材料与绿色制造技术工业和信息化部重点实验室, 哈尔滨 150001; 3. 华润水泥技术研发有限公司, 广州 510000; 4. 陆军装备部驻北京地区第一军代处, 北京 100072; 5. 中国航天科工集团第四研究院第四总体设计部, 北京 100048; 6. 哈尔滨工业大学(深圳) 材料科学与工程学院, 深圳 518055)

摘 要: *h*-BN 陶瓷以其良好的热稳定性和优异的介电性能而成为高超声速飞行器防热透波部件的优异材料, 然而 *h*-BN 陶瓷烧结致密化相对困难, 且力学性能较差。$SrAl_2Si_2O_8$ (SAS)具有较低的熔点和较高的强度, 将其引入到 *h*-BN 陶瓷中能够起到促进烧结和补强增韧的作用。本研究以 *h*-BN、$SrCO_3$、Al_2O_3 和 SiO_2 为原料, 采用热压烧结制备了 BN-SAS 复相陶瓷, 研究了烧结压力对复相陶瓷显微组织结构、力学性能和热学性能的影响规律, 并评价了 BN-SAS 复相陶瓷的抗热震性能。结果表明, 热压烧结制备的 BN-SAS 复相陶瓷的物相主要为六方氮化硼和六方锶长石。随着烧结压力增大, 复相陶瓷的致密度增加, 力学性能呈现先增大后略有降低的趋势。在 20 MPa 烧结压力下制备的复相陶瓷的力学性能最优, 其抗弯强度和断裂韧性分别为(138±4) MPa 和(1.84±0.05) $MPa·m^{1/2}$。10 MPa 烧结压力下制备的 BN-SAS 复相陶瓷具有较低的热膨胀系数, 在 200~1200 ℃范围内的平均热膨胀系数为 $2.96×10^{-6}$ K^{-1}。20 MPa 烧结压力下制备的复相陶瓷的热导率较高, 室温~1000 ℃时热导率变化范围为 12.42~28.42 $W·m^{-1}·K^{-1}$。BN-SAS 复相陶瓷表现出良好的抗热震性能, 经 600~1400 ℃温差的热震实验后, 其残余抗弯强度先增大后迅速降低。复相陶瓷的残余抗弯强度在热震温差为 800 ℃时达到最高, 残余强度保持率为 101%。随着热震温差逐渐增大, 陶瓷表面的氧化程度逐步加剧, 热应力引起的裂纹逐渐增多。

关 键 词: BN 基复相陶瓷; 热压烧结; 力学性能; 抗热震性; 服役可靠性

中图分类号: TQ174 **文献标志码:** A **文章编号:** 1000-324X(2024)10-1182-07